AGU PUBLICATIONS

JGR

Journal of Geophysical Research: Solid Earth

RESEARCH ARTICLE
10.1002/2016JB012818

Key Points:
- Maximum induced earthquake magnitudes are consistent with Gutenberg-Richter sampling statistics
- The number of induced earthquakes is verified to scale as the volume of fluid injected
- Mmax for induced earthquakes is likely the same as for similarly located tectonic earthquakes

Supporting Information:
- Supporting Information S1

Correspondence to:
N. J. van der Elst,
nvanderelst@usgs.gov

Citation:
van der Elst, N. J., M. T. Page, D. A. Weiser, T. H. W. Goebel, and S. M. Hosseini (2016), Induced earthquake magnitudes are as large as (statistically) expected, *J. Geophys. Res. Solid Earth*, *121*, 4575–4590, doi:10.1002/2016JB012818.

Received 12 JAN 2016
Accepted 12 JUN 2016
Accepted article online 15 JUN 2016
Published online 30 JUN 2016

Induced earthquake magnitudes are as large as (statistically) expected

Nicholas J. van der Elst[1], Morgan T. Page[1], Deborah A. Weiser[1,2], Thomas H.W. Goebel[3], and S. Mehran Hosseini[4]

[1]U.S. Geological Survey Earthquake Science Center, Pasadena, California, USA, [2]Department of Earth, Planetary, and Space Sciences, University of California, Los Angeles, California, USA, [3]Department of Earth and Planetary Science, University of California, Santa Cruz, California, USA, [4]Mork Family Department of Chemical Engineering and Materials Science, University of Southern California, Los Angeles, California, USA

Abstract A major question for the hazard posed by injection-induced seismicity is how large induced earthquakes can be. Are their maximum magnitudes determined by injection parameters or by tectonics? Deterministic limits on induced earthquake magnitudes have been proposed based on the size of the reservoir or the volume of fluid injected. However, if induced earthquakes occur on tectonic faults oriented favorably with respect to the tectonic stress field, then they may be limited only by the regional tectonics and connectivity of the fault network. In this study, we show that the largest magnitudes observed at fluid injection sites are consistent with the sampling statistics of the Gutenberg-Richter distribution for tectonic earthquakes, assuming no upper magnitude bound. The data pass three specific tests: (1) the largest observed earthquake at each site scales with the log of the total number of induced earthquakes, (2) the order of occurrence of the largest event is random within the induced sequence, and (3) the injected volume controls the total number of earthquakes rather than the total seismic moment. All three tests point to an injection control on earthquake nucleation but a tectonic control on earthquake magnitude. Given that the largest observed earthquakes are exactly as large as expected from the sampling statistics, we should not conclude that these are the largest earthquakes possible. Instead, the results imply that induced earthquake magnitudes should be treated with the same maximum magnitude bound that is currently used to treat seismic hazard from tectonic earthquakes.

1. Introduction

1.1. The Maximum Magnitude of Induced Earthquakes

The recent surge of small to moderate magnitude earthquakes in the central and eastern U.S., as well as in parts of Europe, has attracted considerable attention [*Keranen et al.*, 2013; *Frohlich et al.*, 2011; *Frohlich*, 2012; *Frohlich et al.*, 2014; *Horton*, 2012; *Rubinstein et al.*, 2014; *Friberg et al.*, 2014; *Holland*, 2013; *Kim*, 2013; *Hornbach et al.*, 2015; *van Thienen-Visser and Breunese*, 2015] and has prompted a reconsideration of seismic hazard in regions of formerly small concern [*Petersen et al.*, 2015]. Little controversy remains regarding the connection between earthquakes and deep injection from wastewater disposal and secondary oil recovery [*National Research Council*, 2013]. However, key questions remain about how to assess the hazard from these earthquakes. One of the most important questions is whether there is a deterministic limit on the maximum size of an induced earthquake that differs from the limit on tectonic earthquakes in the same location.

It has been suggested that the size of the largest induced earthquakes may be limited by the size of the stimulated reservoir [*Shapiro et al.*, 2007, 2010, 2011] or by the total amount of fluid injected [*McGarr*, 1976, 2014; *Hallo et al.*, 2014]. However, these studies generally admit that deterministic limits should not apply if the earthquakes are free to propagate along faults outside the injection reservoir. If induced earthquakes occur on tectonic faults, and are fueled primarily by tectonic strain energy, then the intrinsic limit on magnitude may be set only by the tectonics. The magnitude bound for tectonic earthquakes is notoriously difficult to constrain from observed seismicity alone [*Holschneider et al.*, 2011] and instead relies on considerations of the extent—and in particular, the connectivity—of regional faults, which is beset by its own substantial uncertainty [*Mignan et al.*, 2015]. In the absence of clear evidence supporting either the tectonic or reservoir limit, current approaches resort to logic trees with somewhat subjectively weighted branches [*Petersen et al.*, 2015; *Mignan et al.*, 2015b].

New observations of relatively long-range (>10 km) interactions between wells and induced earthquakes [*Keranen et al.*, 2014; *Block et al.*, 2014; *Goebel et al.*, 2015] suggest that induced earthquakes are not as tightly

confined to the immediate injection reservoir as previously hoped [*Davis and Frohlich*, 1993]. Likewise, the recognition that earthquake-earthquake triggering can amplify induced seismicity rates through cascading [*Baisch et al*., 2006; *Llenos and Michael*, 2013; *van der Elst et al*., 2013; *Sumy et al*., 2014] suggests that an earthquake initiated by a pore pressure perturbation may not be entirely confined to the volume affected by that perturbation. While there is evidence that the size of microearthquakes induced in some special cases is limited by the geometry and fracture distribution of the host formation [*Eaton et al*., 2014], it remains to be demonstrated that induced earthquakes in general (and large induced earthquakes in particular) are physically distinct from tectonic earthquakes.

In this study, we start with the hypothesis that induced earthquakes have the same magnitude limit as tectonic earthquakes and set about trying to disprove this hypothesis. While the absolute maximum magnitude of tectonic earthquakes is generally hard or impossible to determine from statistics alone [*Holschneider et al*., 2014], it is relatively straightforward to compute the expected maximum magnitude within any finite sample of earthquakes—e.g., a swarm of induced earthquakes.

Tectonic earthquakes generally follow the Gutenberg-Richter (GR) magnitude-frequency distribution (MFD) [*Ishimoto and Iida*, 1939; *Gutenberg and Richter*, 1944]. If magnitudes are drawn randomly from the GR distribution, the probability of sampling a magnitude in excess of a given value increases with sample size. The question we pose for induced seismicity is whether the largest observed magnitudes are consistent with the sampling statistics of the Gutenberg-Richter MFD, given the total number of induced earthquakes at each site. We will refer to this as the "sample size" hypothesis for maximum magnitude.

To evaluate the sample size hypothesis, we first derive the basic expressions for the largest expected earthquake in a sample of size N. We then show that the data compiled by *McGarr* [2014]—which were taken to support a deterministic upper magnitude limit—are consistent with the sample size hypothesis, as long as the number of induced earthquakes is proportional to volume injected.

For a more definitive evaluation, we develop and test three predictions of the sample size hypothesis: (1) The maximum observed magnitude is a function of the number of prior induced earthquakes; (2) the order of occurrence of the largest earthquake is random within the sequence (each earthquake has the same probability of being the largest); and (3) the number of induced earthquakes is proportional to the volume injected.

The first test establishes whether we should expect to have seen any larger earthquakes given the total sample size. The second test establishes whether the magnitudes of the induced earthquakes are actually dependent on the injection history. The third test is not strictly required by the sample size hypothesis, but it is expected to hold if fluid injection controls earthquake nucleation rather than earthquake size. This would be consistent with the way we think about other kinds of triggered earthquakes, e.g., aftershocks [*Helmstetter et al*., 2005].

If the data pass all three tests, then the largest induced earthquakes are exactly as large as expected given the length of the observation interval. We must then be very cautious about any physical model that concludes that the largest possible earthquake is already present in the sample. It may instead be more prudent to act under the assumption that induced earthquake magnitudes have the same intrinsic limit as similarly located tectonic earthquakes do, such that a longer observation window (with continued injection) may turn up additional rare large events.

2. Methods

2.1. Probabilistic M_{max} Based on Sample Size

McGarr [2014] compiled a number of high-profile cases of induced seismicity to argue for a deterministic cap on the seismic moment of induced earthquakes, set by the injection volume. These sites were chosen based on the relative simplicity of the injection history, clarity of the association between earthquakes and injection, and the availability of existing seismic analyses in the scientific literature. Under a particular set of assumptions—including the assumption that induced earthquakes do not rupture outside the hydraulically perturbed volume—*McGarr* [2014] derived a limit on induced earthquake moment M_0 equal to $M_0 = G\Delta V$, where G is the shear modulus and ΔV the total injected volume. This implies that $M_w = (2/3)\log_{10} M_0 - 6$, according to the definition of moment magnitude [*Hanks and Kanamori*, 1979]. The observed cases of

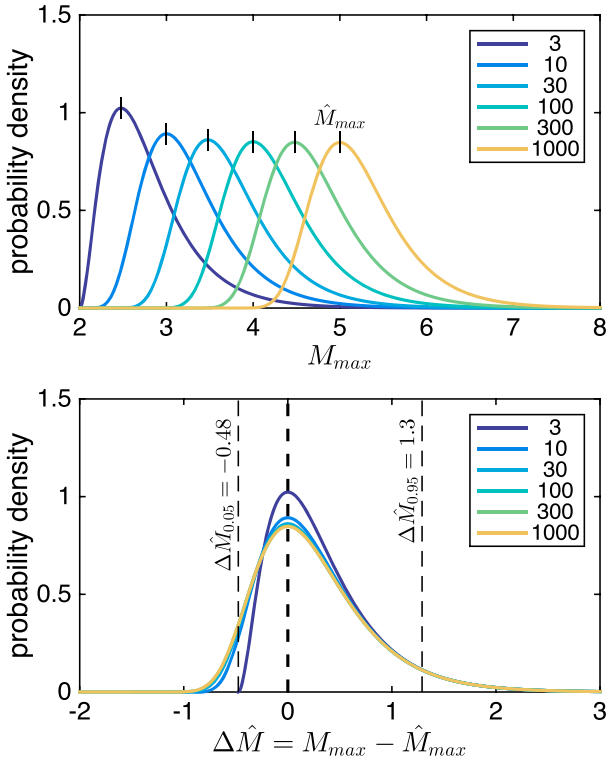

Figure 1. Probability density functions for maximum observed magnitude as a function of sample size *N*. (top) The mode for each distribution (equation (1)) is marked by a vertical tick. (bottom) The pdfs aligned on the mode, showing curve collapse for $N > 10$. Vertical dashed lines give 90% confidence bounds from equation (2).

induced seismicity seem to respect this upper bound so far [*McGarr*, 2014]. The fundamental question in this paper is whether we would expect any earthquakes to exceed this bound given the sampling statistics of the Gutenberg-Richter distribution and given the total number of induced earthquakes observed so far.

Here we derive an alternative expectation for the maximum magnitude $M_{\max}$ based on sample size statistics. For brevity we present only those equations required to illustrate the basic scaling of maximum magnitude with sample size and the final equation used to test the sample size prediction. A more complete derivation is found in Appendix A.

If earthquakes follow a Gutenberg-Richter distribution, i.e., exponentially distributed in magnitude, then the most probable maximum magnitude to be observed in a sample of size *N* is

$$\widehat{M}_{\max} = M_c + \frac{1}{b}\log_{10} N, \tag{1}$$

where *b* is the slope of the power law, M_c is a reference magnitude, and *N* is the number of earthquakes observed above magnitude M_c (Appendix A). Equation (1) corresponds to the mode of the distribution of $M_{\max}$ (Figure 1). (Note that this equation can be obtained quite simply by setting $N = 1$ in the Gutenberg-Richter equation.)

The distribution for $M_{\max}$ is heavy tailed, just like the GR distribution. We can invert the cumulative density function of $M_{\max}$ (Appendix A) to get bounds on the expected maximum magnitude,

$$\widehat{M}_q = \widehat{M}_{\max} - \frac{1}{b}\log_{10}\left[N\left(1 - q^{1/N}\right)\right], \tag{2}$$

where $\widehat{M}_q$ is the magnitude corresponding to some confidence level *q*. In the limit of large *N* or *q* close to one, equation (2) simplifies to

$$\widehat{M}_q = \widehat{M}_{\max} - \frac{1}{b}\log_{10}(-\ln q), \tag{3}$$

Assuming $b = 1$, equation (3) predicts that 90% of the maximum magnitude observations should fall between -0.48 and $+1.3$ magnitude units of the mode $\widehat{M}_{\max}$ given by equation (1).

Equations (1)–(3) constitute the core of the sample size hypothesis. However, to compare the sample size prediction to the scaling observed by McGarr, we must first connect the number of triggered events to total injected volume. The number of earthquakes triggered by fluid injection is commonly parameterized in terms of the seismogenic index Σ,

$$\log_{10}(N) = \Sigma + \log_{10} V - bM_c, \tag{4}$$

where *V* is the volume injected. This formula is common in geothermal applications, where the seismogenic index is found to be relatively constant over the lifetime of the reservoir [*Shapiro et al.*, 2010, 2011] and is supported by studies of injection-induced seismicity [*Shapiro et al.*, 2007; *Rubinstein et al.*, 2014; *Asanuma et al.*, 2005].

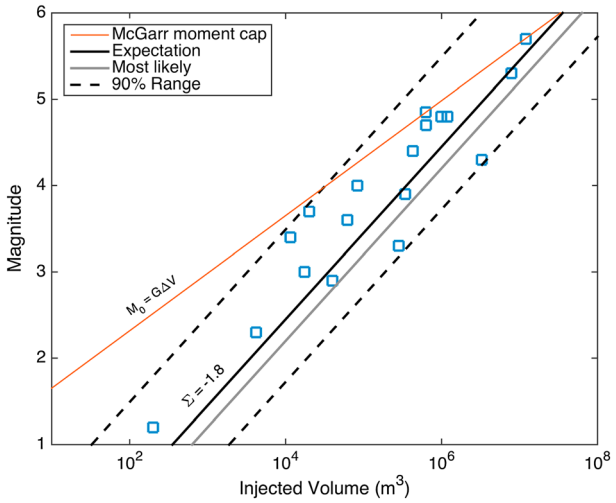

Figure 2. Maximum observed magnitude versus total injected volume, at a number of fluid injection sites reproduced from Table 1 of *McGarr* [2014]. McGarr's moment cap is shown by the orange line, while the statistical expectation and its 90% probability bounds (equation (3)) are given by the black solid and dashed lines, respectively, (assuming $b = 1$ and $\Sigma = -1.8$). The mode of the distribution equation (5) is given by the somewhat lower gray line.

Equation (4) implies that the total number of induced earthquakes is proportional to injection volume. We will confirm this in subsequent sections, but for now we take it as an assumption and combine equations (1) and (4) to get a simple expression for the maximum magnitude as a function of injected volume.

$$\widehat{M}_{\max} = \frac{1}{b}(\Sigma + \log_{10} V). \tag{5}$$

This estimate has the same confidence bounds as given by equations (2) and (3).

To check that we are on the right track, i.e., that the sample size hypothesis can plausibly explain the data, we plot the sample size prediction for maximum magnitude (equation (5)) in Figure 2, using a hypothetical seismogenic index of $\Sigma = -1.8$, chosen to fit the data. The statistical scaling matches the scaling of the data quite well, including at lower injection volumes where the moment cap significantly exceeds the observed maximum magnitudes. The comparison shows that the sample size hypothesis is a plausible explanation for the observations but does not constitute a rigorous test (because it includes Σ as a free parameter). In the following sections we test the three predictions of the sample size hypothesis independently, using no adjustable parameters.

2.2. Probabilistic M_{max} When the True Sample Size Is Unknown

To test the prediction that the largest earthquake at each site is determined by the sample size (Prediction 1), we need three measurements: the number N of induced earthquakes prior to the largest event, the b value, and the magnitude of completeness M_c at each site. Technically, we could use any reference magnitude in place of M_c, but we choose M_c in order to use all of the information available in the sample. Equations (1) and (2) then give us the most likely maximum magnitude $\widehat{M}_{\max}$ and its confidence bounds.

If we were making a prospective forecast, equations (1) and (2) would be sufficient to make a statement about the largest event we expect out of N_{tot} future events. The current analysis, however, is retrospective—the largest earthquake has already occurred. To make sure that our statistics are independent of the largest earthquake itself, we count only the number of events N prior to the largest earthquake. However, this conditions the event count on the order of occurrence of the largest event. Since N is necessarily less than or equal to N_{tot}, N will necessarily underpredict M_{max}.

We can correct for this conditioning by recognizing that N is a uniform random variable. Prediction 2 of the sample size hypothesis states that the largest earthquake can fall anywhere within the sample, because all magnitudes are drawn from the same stationary GR distribution. The number of events N prior to the largest event is thus a discrete uniform variable on the interval $[1, N_{tot}]$. The deviation $\Delta M_{\max}$ between the true sample maximum (assuming N is uniform) and the naïve estimate (i.e., assuming $N = N_{tot}$) has the distribution

$$f_{\Delta M_{\max}}(\Delta m | N_{\text{tot}}) = b\ln(10)\cdot 10^{-b\Delta m} \sum_{N=N_{\min}}^{N_{\text{tot}}} \frac{1}{N}\left[1 - \frac{1}{N}10^{-b\Delta m}\right]^{N_{\text{tot}}-1}, \tag{6}$$

where the lower limit of the summation is $N_{\min} = 10^{-b\Delta m}$ (Appendix A). The bias-corrected estimate of the most likely maximum magnitude is

$$\widehat{M}'_{\max} = \widehat{M}_{\max} + \langle \Delta M_{\max} \rangle. \tag{7}$$

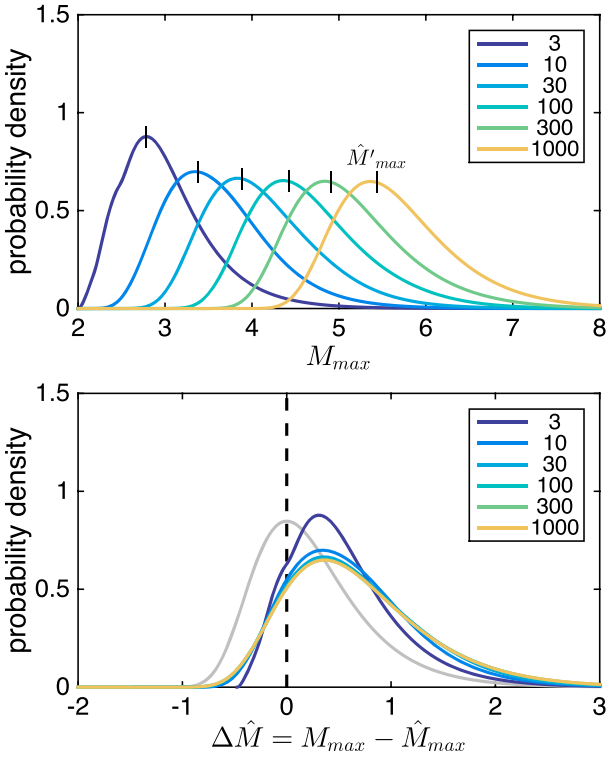

Figure 3. (top) Probability density functions for maximum observed magnitude as a function of the number of prior events N, given that the true sample size N_{tot} is unknown. (bottom) Distribution of ΔM_{max} (equation (6)) relative to the naïve prediction based on N (equation (1)). The gray curve is the distribution of M_{max} under the assumption that $N = N_{tot}$ (from Figure 1).

In the limit of large N_{tot}, the bias-corrected maximum $\hat{M}'_{max}$ is $\log_{10}(e) \approx 0.4$ units larger than the naïve maximum $\hat{M}_{max}$ (Appendix A).

To be consistent with our decision to not use sample information from after the largest event, the upper bound N_{tot} must also be treated as an unknown. Fortunately, Prediction 3, where the number of earthquakes is proportional to volume, gives us an estimate of the form $\hat{N}_{tot} = NV_{tot}/V$, where V and V_{tot} are the injected volumes at the time of events N and N_{tot}, respectively. It turns out that as long as $\hat{N}_{tot}$ is fairly large (>25), the distribution of ΔM_{max} depends very little on $\hat{N}_{tot}$ (Figure 3). Equation (6) is the foundation for testing Prediction 1 of the sample size hypothesis.

2.3. Catalogs

To prevent selection bias, we restrict the analysis to only those sites included in the compilation by *McGarr* [2014] (Table 1). At two of the sites (Soultz-sous-Forêts and Cooper Basin, Australia) we separated the catalogs into distinct stimulation episodes. Both of these sites are Enhanced Geothermal Stimulation (EGS) projects, with successive stimulations separated by several years. Treating each of the episodes as an additional data point adds more power to the statistical tests, but all of our conclusions continue to hold if we were to treat these sites as single data points.

Table 1. Site and Source Descriptions

Site	Full Name	Type	Earthquake/Injection References
KTB	KTB borehole	Scientific	*Jost et al.* [1998] and *Zoback and Harjes* [1997]
BUK	Bowland Shale, UK	Hydraulic Frac.	*Eisner et al.* [2011] and *de Pater and Baisch* [2011]
GOK	Garvin, OK	Hydraulic Frac.	*Holland* [2013] (matched filter)
SZ1-4	Soultz (GPK-2,3,4)	EGS	*Charlety et al.* [2007] (hand digitized to M 1.7 for SZ1 and to M 1.4 for SZ2-4)
DFW	Dallas Fort Worth	Wastewater	*Frohlich et al.* [2011] (matched filter); Texas Railroad Commission
BAS	Basel, Switzerland	EGS	Swiss Seismol. Service (SED); *Häring et al.* [2008] and *Bachmann et al.* [2011]
A87	Ashtabula, OH 1987	Wastewater	ComCat; *Seeber et al.* [2004]; Ohio Seismic Network
CB1-4	Cooper Basin, Aus.	EGS	Geoscience Australia; *Asanuma et al.* [2005] and *Baisch et al.* [2006, 2009, 2015]
A01	Ashtabula, OH 2001	Wastewater	ComCat; *Seeber et al.* [2004]
YOH	Youngstown, OH	Wastewater	[*Kim*, 2013] (matched filter)
PDX	Paradox Valley	Wastewater	PVSN Annual Reports 1998–2013; *Ake et al.* [2005]
R01	Raton Basin, 2001	Wastewater	*Rubinstein et al.* [2014]; Colorado Oil and Gas Conservation Commission
R11	Raton Basin, 2011	Wastewater	
GUY	Guy-Greenbriar, AR	Wastewater	ComCat; *Horton* [2012]; Arkansas Oil and Gas Commission
POH	Painsville, OH	Wastewater	ComCat; Ohio Seismic Network
TTX	Timpson, TX	Wastewater	*Frohlich et al.* [2014]; Texas Railroad Commission
RMA	Rocky Mountain Arsenal	Wastewater	CEUS Seismic Source Characterization; *Evans* [1966] and *Hsieh and Bredehoeft* [1981]
POK	Prague, OK	Wastewater	ComCat; *Keranen et al.* [2013]; Oklahoma Corporation Commission
HAR	Harrison, OH	Hydraulic Frac.	*Friberg et al.* [2014] (matched filter)
GDF	Goodfellow	Laboratory	*Goodfellow et al.* [2015]

Table 2. Summary of Induced Earthquake Sequences

Site	M_{max}[a]	M_{exp}[b]	N	N_{tot}	V (m^3)	V_{tot} (m^3)	b	M_c	M_{GV}[c]
KTB	1.2	0.8	33	70	1*e*2	2*e*2	1.3	−1.0	2.1
BUK	2.3	2.1	11	23	4.1*e*3	8.4*e*3	1.0	0.1	3.4
GOK[d]	2.9	3.3	14	20	1.8*e*4	3.5*e*4	1.4	1.9	3.8
SZ1[g]	2.6	3.1	75	75	2.3*e*4	2.3*e*4	1.7	1.7[e]	3.9
SZ2[g]	2.9	4.3	92	106	3.3*e*4	3.3*e*4	1.0	1.8[e]	4.0
SZ3[g]	2.3	2.2	14	21	8.5*e*3	8.5*e*3	2.1	1.4[e]	3.6
SZ4[g]	2.6	2.1	2	21	7.4*e*3	1.2*e*4	1.3	1.4[e]	3.6
DFW[d]	3.3	3.9	69[e]	88	3.8*e*5	5*e*5	1.3[e]	2.0[e]	4.7
BAS	3.4	3.2	109	188	1.2*e*4	1.2*e*4	1.3	1.2	3.7
A87	3.5	3.5	1	9	6*e*4	3.4*e*5	1.1	2.4	4.2
CB1	3.7	4.1	4	11	8.9*e*3	2.3*e*4	1.0	2.6	3.6
CB2	2.9	-	-	-	-	2.2*e*4	-	-	-
CB3	1.6	-	-	-	-	3.8*e*2	-	-	-
CB4	3.0	-	-	-	-	3.4*e*4	-	-	-
A01	3.9	4.0	20	27	3.4*e*5	3.4*e*5	1.1	2.4	4.7
YOH[d]	3.9	3.3	94	95[e]	7.9*e*4	7.9*e*4	1.0	0.7	4.2
PDX	4.3	5.0	836	1454	2.7*e*6	7.8*e*6	1.0	1.0	5.3
R01	4.4	5.4	6	53	4.6*e*5	7.8*e*6	1.2	3.4	4.8
R11	5.3	5.1	46	53	7.8*e*6	7.8*e*6	1.2	3.4	5.6
GUY	4.7	4.7	285	298	4.1*e*5	5.6*e*5	1.2	2.2	4.7
POH	5.0	3.0	2	2	1.2*e*6	1.2*e*6	1.0[f]	2.7[e]	5.0
TTX	4.8	4.1	2	4	1*e*6	1.2*e*6	0.6[e]	3.0[e]	5.0
RMA	5.3	5.7	20	25	6.2*e*5	6.2*e*5	1.3	4.3	4.8
POK	5.6	4.5	8	34	6.7*e*6	7.8*e*6	1.2	3.3	5.5
HAR[d]	2.1	3.1	182	220	7*e*4	9.4*e*4	1.0	0.3	4.2
GDF	−7.0	-	-	-	-	4.2*e*−6	-	-	-

[a]Observed largest earthquake sequence.
[b]Expected largest earthquake (equation (A14)).
[c]Deterministic maximum magnitude based on injection volume ($M_0 = G\Delta V$).
[d]Matched filter catalog.
[e]Value taken from reference.
[f]Typical value for region.
[g]Hand digitized.

For each site, we determine the number of prior and total events N, the b value and the magnitude of completeness M_c (Table 2). To test the scaling between number and volume, we also measure the injected volume V at the time of the largest event and the total injected volume V_{tot}. The earthquake data come from regional networks, temporary deployments, and matched-filter analyses (Table 1). The earthquake catalogs taken from the literature extend beyond the end of injection and are assumed to capture the entirety of the induced sequences. While it is possible that much later earthquakes are related to earlier injection activities, it would be difficult to prove this connection and provide an unfair test of the moment cap hypothesis. We therefore restrict our analysis to the sequences as described in the primary sources. In cases where the sequence is still ongoing (e.g., Paradox Valley), we include the most recent data available as of November 2015. Magnitudes are as reported in the catalogs. As such, the magnitudes may not be perfectly calibrated to conventional moment magnitudes. While more accurate moment magnitudes likely exist in other sources for some of the larger earthquakes, we restrict ourselves to the catalog magnitudes in order to avoid potential errors introduced by switching magnitude scales between large and small earthquakes. Injection volumes come from state regulatory agencies for most sites in the U.S. or from the literature. In a few cases, we resort to hand-digitizing earthquake or injection data directly from figures. Data sources for each site are summarized in Table 1. (For more details on compiling the data, see "Notes on Analysis" included in the supporting information to this article.)

2.4. Magnitude of Completeness and *b* Value

Whenever the data permit, we estimate the catalog completeness M_c using the method of *Clauset et al.* [2009]. This is a relatively conservative approach, based on a Kolmogorov-Smirnoff goodness of fit comparison to the assumed GR distribution. This ensures that the calculated b value is in fact a good description of the

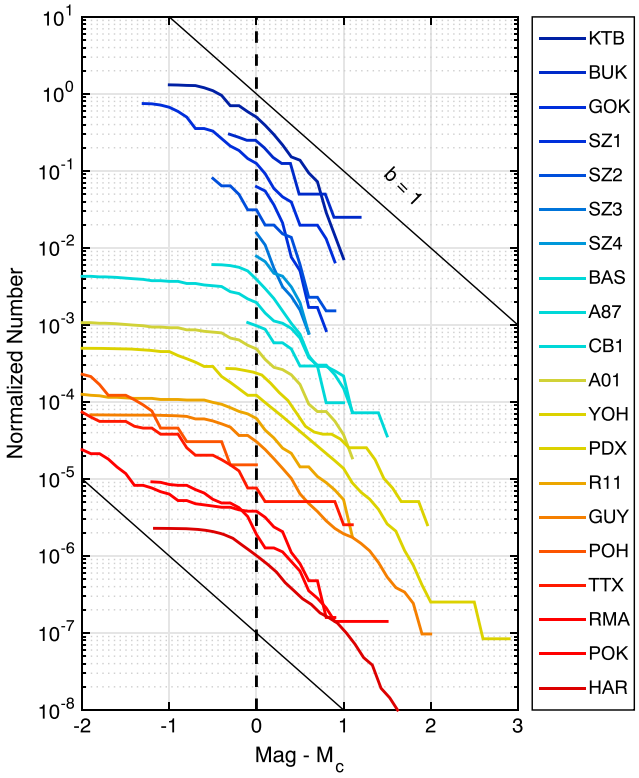

Figure 4. Magnitude-frequency distributions for all sites, aligned on M_c. Curves are offset vertically for clarity.

earthquakes in the sample (Figure 4). The *b* value is estimated by maximum likelihood [*Aki*, 1965], with corrections for magnitude rounding [*Shi and Bolt*, 1982].

At some sites we do not have the actual earthquake catalog (Tables 1 and 2), or there are insufficient data to estimate the *b* value with the method of *Clauset et al.* [2009] (we require at least 0.5 magnitude unit between M_c and the second largest earthquake in the sample). In these cases, we take the *b* value listed in the corresponding literature.

3. Results

3.1. Test 1: M_{max} Is Predicted by the Number of Prior Events

We find strong agreement between the observed maximum magnitudes M_{max} and the magnitudes expected based on *b* value, the completeness magnitudes, and the number of prior events (Figure 5a). The majority of the earthquakes fall within the 90% confidence range of the expected distribution (equation (6)). This is a direct consequence of the scaling between maximum observed magnitude and number of prior earthquakes (Figure 5b).

The most prominent outliers in Figure 5 are the Painsville, Ohio, earthquake on the highside (POH) and the second of four stimulations at Soultz on the lowside (SZ2). It should be noted that the statistics used in the Painsville, Ohio, prediction are the least well-constrained in the entire study (Table 1). Disregarding point POH, the earthquake that most exceeds the expected magnitude is the 2011 M_W 5.6 Prague earthquake.

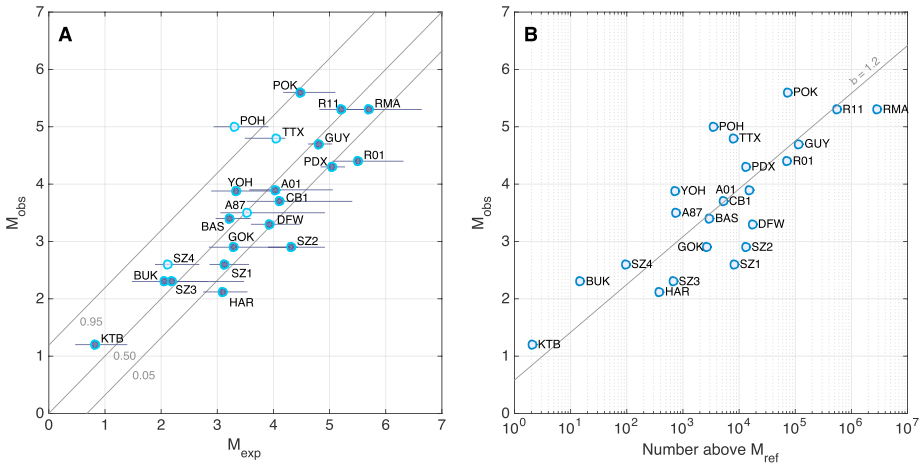

Figure 5. (a) Observed versus expected maximum magnitude M_{max}. Diagonal lines are probability contours for the expected maximum (equation (6)) assuming $b = 1.2$. Thin horizontal lines show 95% confidence ranges associated with *b* value uncertainty at each site. Pale circles have two or fewer earthquakes in the sample and may be unreliable. (b) Observed M_{max} as a function of the number of prior events above a reference magnitude $M_{ref} = 0$, assuming $b = 1.2$.

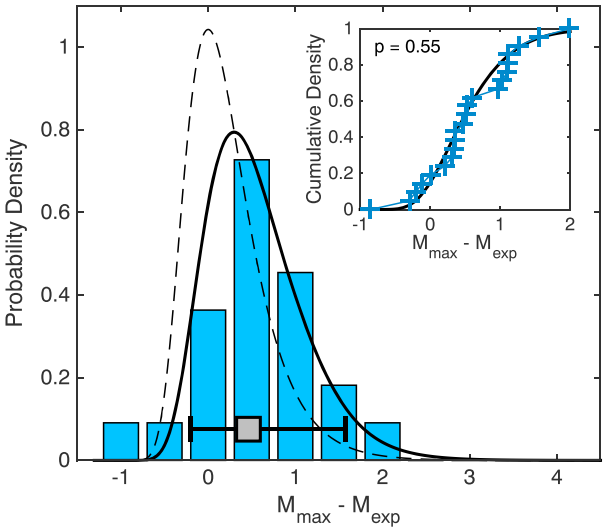

Figure 6. Distribution of the difference between the observed M_{max} and the prediction based on the number of prior events N (equation (1)). The dashed black line is the expected distribution if N were the full sample size; the bold line takes into account the reality that N prior is necessarily smaller than the true sample size (equation (6)). The whisker plot marks the median and 90% confidence range. (inset) Empirical (plus sign) and predicted cumulative density functions. The reported $p = 0.55$ is for the Kolmogorov-Smirnoff goodness of fit test.

Despite some outliers (e.g., SZ2), the distribution of observed maximum magnitudes closely follows that expected from equation (6) (Figure 6). The Kolmogorov-Smirnoff goodness of fit test gives $p = 0.55$, meaning that over half of random samples drawn directly from the assumed distribution would actually fit less well than the observations. The maximum observed magnitudes of induced earthquakes are consistent with the sampling statistics, given the number of prior induced earthquakes at each site and no assumed upper limit on magnitude.

3.2. Test 2: The Order of the Largest Earthquake Is Random

The second test bears directly on the issue of whether the magnitude of the largest earthquake is controlled by the size of the pressure perturbation. The moment cap model holds that the largest possible earthquake increases with the total volume injected, with the larger earthquakes preferentially occurring late within the sequence. The sample-size hypothesis holds that each earthquake in the sequence has the same probability of becoming the largest, regardless of the order in which it occurs, because the size is determined by the tectonics—not by the size of the perturbation that started it.

Figure 7 shows the order of occurrence of the largest events, expressed as the ratio of prior events to total events in the sequence. The order of occurrence of the largest earthquakes is indeed consistent with the sample-size hypothesis, with $p = 0.30$ (Figure 7).

While a uniform order of occurrence clearly cannot be rejected ($p = 0.30$), the agreement between the observations and the statistical model is not as compelling as it was for Test 1 (Figure 6). In 13 out of 22 cases, the largest event falls within the latter half of the sequence. This is only two more than expected (with a probability of occurring by chance of 16%) but could be taken as evidence that the largest possible magnitude indeed grows with time and volume injected. However, this trend disappears if we exclude those cases where injection operations were actually halted because of large induced events: Basel; Youngstown, Ohio; Guy, Arkansas; and the Rocky Mountain Arsenal [*Häring et al.*, 2008; *Kim*, 2013; *Horton*, 2012; *Hsieh and Bredehoeft*, 1981]. In these instances, the order of occurrence of the largest event is strongly biased by the decision to halt injection.

Excluding cases affected by operator bias, we find the remaining events to be uniformly distributed, with $p = 0.68$. This is now a satisfying fit; fewer than half of samples drawn directly from a uniform distribution would be expected to fit as well as the observations. The data therefore again support the hypothesis that induced earthquake magnitudes are drawn independently from a Gutenberg-Richter distribution rather than being physically determined by increasing injection volumes.

3.3. Test 3: The Number of Induced Earthquakes Is Proportional to Volume

The third prediction, as discussed above, is not fundamental to the sample size hypothesis but is necessary to explain the apparent scaling of M_{max} with $\log_{10}V$ (Figure 2).

We find that the number of earthquakes is indeed proportional to the total volume injected (Figure 8), both at the time of the largest earthquake and at the end of the induced sequence. We again scale all numbers to an arbitrary reference magnitude $M_{ref} = 0$, assuming $b = 1.2$ (the median value). The total number of induced earthquakes at the time of the largest event increases linearly with volume injected, with some scatter attributable to

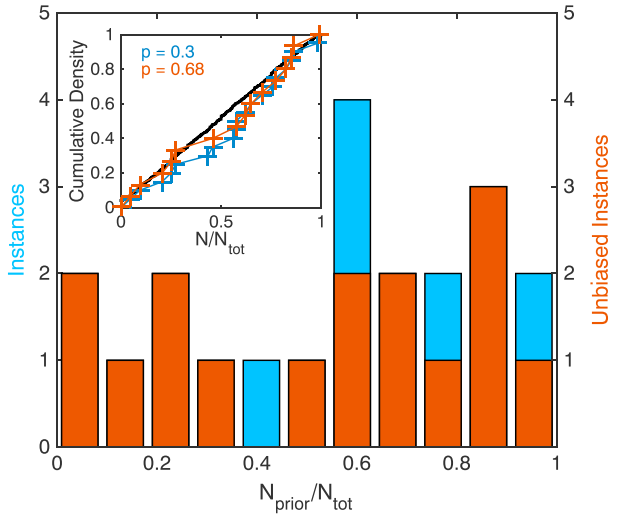

Figure 7. Distribution of the order of occurrence of the largest earthquakes. The distribution should be approximately uniform if magnitudes are independent and identically distributed. Red histogram excludes biased cases where operators shut down injection because of a large earthquake. (inset) Empirical (plus sign) and predicted cumulative density functions.

variability in the seismogenic index (Figure 8). For sequences in which the largest event came relatively early, we find that the number of post largest event earthquakes also grows more or less linearly with the post largest event injection volume (Figure 8, green lines).

Linear scaling is in fact the best predictor of the relation between future injection volume and future earthquake number. In functional form we have

$$N_{pred} = N(V_{tot}/V)^n, \quad (7)$$

which we used in equation (6) (with $n = 1$) to estimate the total number of events in the sequence N_{tot} based only on the number N prior to the largest event. The best prediction of N_{tot}, in terms of minimizing the variance of $\log(N_{pred}/N_{tot})$, is obtained for $n = 0.96$, insignificantly different from $n = 1$ (Figure 9).

3.4. Summary: M_{max} Versus Injected Volume

Finally, we reproduce the maximum magnitude versus volume plot (Figure 10), using catalog magnitudes, which we assume are statistically more consistent with the other earthquakes in each catalog than moment magnitudes but which should not be treated as a test of the deterministic moment cap hypothesis. We also include a few additional data points for individual stimulations at Cooper Basin, which could not be included in other plots due to a lack of timing data on the earthquakes. We confirm that M_{max} is proportional to the logarithm of injected volume V, as must be the case, given the prior observations that $M_{max} \sim \log_{10} N$ (Figure 5b) and $N \sim V$ (Figure 8).

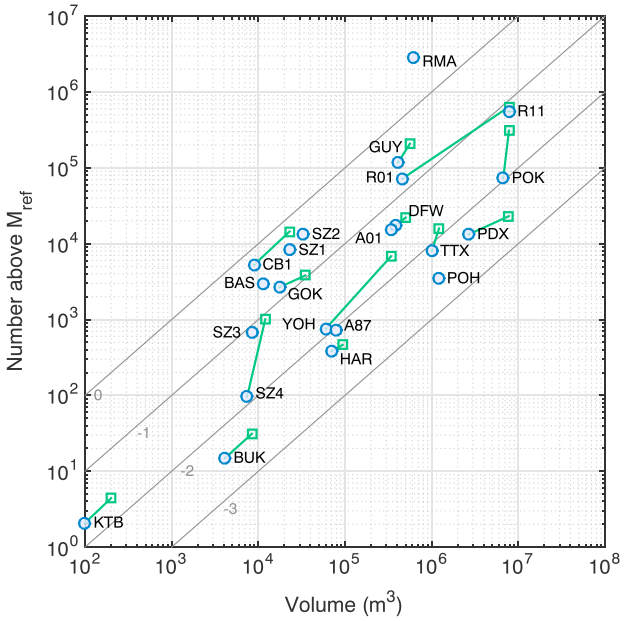

Figure 8. Number of induced earthquakes versus volume, scaled to $M_{ref} = 0$, assuming $b = 1.2$. Blue circles give values at the time of the largest induced earthquakes; connected green squares give final values for that site. Thin gray lines show expected scaling for a range of seismogenic indexes (equation (4)).

While the log of injected volume seems to be a good predictor of maximum magnitude, a definitive demonstration requires observations over a wider range of injection volumes. The smallest induced earthquake we could find in the literature is from a recent experiment involving 4 ml of fluid injected into a sample under triaxial load [*Goodfellow et al.*, 2015]. The resulting lab quakes were shown to have similar source scaling to natural earthquakes (including magnitude independent stress and strain drop), making them valid for comparison. The largest seismic event in the experiment was M_w -7. This event is plotted in the inset of Figure 10 and falls within the range expected for a linear scaling with log of volume, assuming $b = 1.2$. The agreement would be improved somewhat if we assumed $b = 1$ over this wide range of magnitudes.

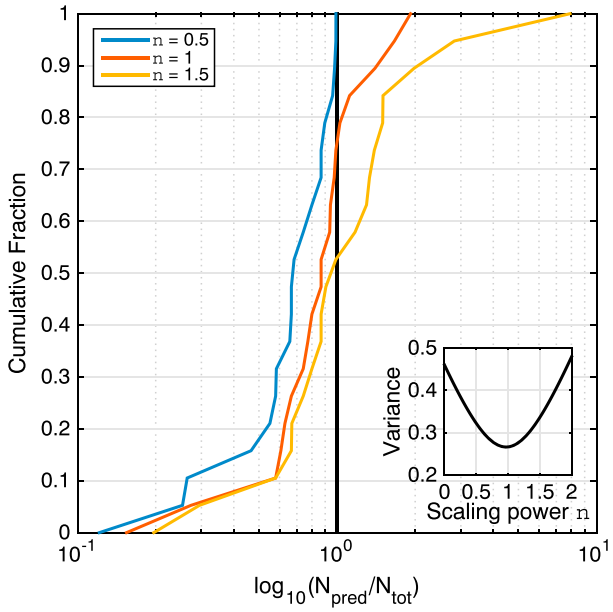

Figure 9. The distribution of the ratio of predicted to observed number of induced earthquakes, using the formula $N_{pred} = N(V_{tot}/V)^n$. N and V are the number of earthquakes and injected volume at the time of the main shock; V_{tot} is the final volume injected at the end of the sequence. (inset) Variance of $\log(N_{pred}/N_{tot})$ as a function of the scaling power n, where N_{tot} is the observed final number of earthquakes. Maximum variance reduction is obtained for an exponent $n = 0.96$.

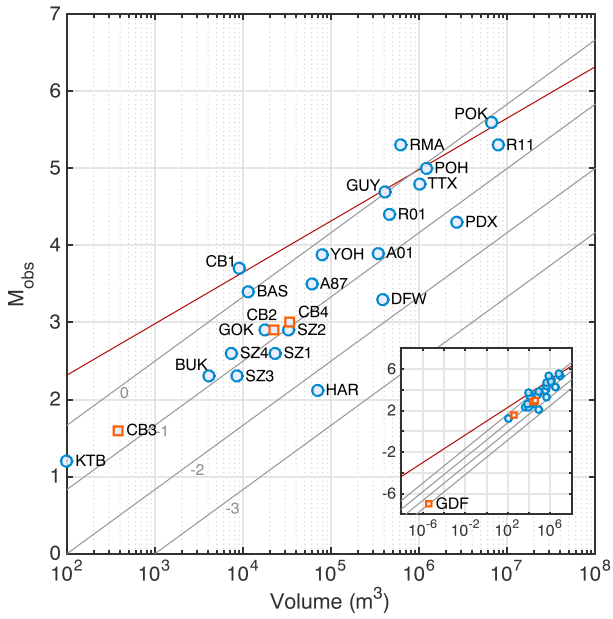

Figure 10. Scaling of the observed M_{max} with injected volume. Thin lines are expected scaling (equation (3)) for different seismogenic indexes, assuming $b = 1.2$. Red line is the moment cap [*McGarr*, 2014] with shear modulus $G = 30$ GPa (note that plotted magnitudes are catalog-preferred magnitudes and not necessarily moment magnitudes). Additional Cooper Basin stimulations have been added as red squares. Inset is zoomed out to include the laboratory observation of *Goodfellow et al.* [2015].

4. Discussion

4.1. Theoretical Justifications for Scaling Between Number and Volume

We found that the volume of injected fluid controls the number of induced earthquakes (Figure 8), rather than controlling the moment of the largest earthquake, at least for the monotonically increasing injection volumes considered here. This is consistent with the idea that the pore pressure perturbation drives earthquake nucleation but that the ultimate size of the triggered earthquake is determined only by the statistics of rupture propagation and arrest on a connected fault network. That is, the probability of inducing an earthquake of a given size is directly related to the probability of encountering—and triggering—an appropriately stressed and tectonically connected nucleation site.

Here we argue that linear scaling between number and volume is consistent with a few simple assumptions about the relationships between injected volume, pore pressure, and triggered nucleation sites. If faults are distributed uniformly away from failure, then the probability of triggering an earthquake at any particular site (assuming faults are present) scales with the local pore pressure increase:

$$N \sim \Delta P. \tag{8}$$

A quasi-uniform distribution of stress from failure is to be expected if the background rate of earthquakes is statistically constant and if tectonic loading is roughly linear in time [*Dieterich*, 1994]. There is evidence from tidal and dynamic triggering of natural earthquakes that faults are indeed uniformly distributed away from failure, at least with respect to small stress perturbations [*Brodsky and van der Elst*, 2014].

Linear poroelasticity requires that the integrated change in pore pressure over the volume of the reservoir scales with the volume of fluid injected [*Wang*, 2000, p110-112],

$$\int_V \Delta P \sim \Delta V. \tag{9}$$

If we assume that the distribution of potential nucleation sites is statistically

homogeneous over the volume explored by the fluid (however heterogeneous that volume), then combining equations (8) and (9) gives

$$\int_V N \sim \int_V \Delta P \sim \Delta V; \tag{10}$$

hence number scales with volume.

This result can be demonstrated rigorously for an isotropic, homogeneous medium [*Shapiro et al*., 2007]. In reality, injection reservoirs are anything but isotropic and homogenous, yet Figure 8 confirms the order of magnitude scaling between volume and number of induced earthquakes both within and between sites, and Figure 9 confirms that linear proportionality gives an optimal forecast of the future number of events.

The simple assumptions underlying equations (8)–(10) may break down on a case-by-case basis. First, there is likely a minimum stress threshold that must be exceeded before equation (8) begins to apply, perhaps set by the level of background stress fluctuations due to tides and seismic waves, the latter of which have triggered earthquakes in injection reservoirs at stress levels of a few kilopascals [*Baisch et al*., 2006; *van der Elst et al*., 2013]. Additionally, since earthquakes relax the preexisting deviatoric stress, there may be diminishing returns as an induced sequence progresses [*Baisch et al*., 2009].

Equation (9) may break down when fully transient poroelastic behavior is considered [*Segall and Lu*, 2015], especially in the presence of reservoir compartments and traps, which may lead to highly nonlinear pore pressure changes as the injection begins to sense the reservoir boundaries [*Keranen et al*., 2013]. Long-range elastic stress transfer may also be important in induced seismicity, allowing earthquakes to be induced outside the region directly affected by pore-fluid diffusion. In this case, the magnitude of the elastic stress change still scales with the pressure change at the injection point and thus with volume injected, and we again expect $N \sim \Delta V$ [*Mignan*, 2016].

Finally, the assumption that nucleation sites are uniformly distributed within the volume explored by the fluid may break down in cases where the injection reservoir is truly isolated from the tectonic fault network, as is the case in many hydrofrack and Enhanced Geothermal Stimulation (EGS) projects or when the injection volume is not large enough to average over the statistical properties of the fault and fracture network. These effects are likely to be most important for short-duration, high-pressure injection operations into unfractured rock, which may explain the possible (but not universal) tendency for the largest event in some EGS operations to follow shut-in by a brief delay [*Baisch et al*., 2010]. These second-order phenomena remain difficult to isolate from the first-order effect of continued pressure diffusion after shut in.

4.2. Discriminating Between the Statistical and Moment Cap Models

We have found little evidence in induced earthquake sequences for a strong cap on maximum magnitude [*McGarr*, 1976, 2014]. Instead, the maximum magnitude appears to be sample size dependent, just as it is for tectonic earthquakes. This should come as no surprise if the induced sequences are occurring on tectonic faults and relaxing tectonic stress. While the total number of induced earthquakes is a function of the total volume injected, the size of the largest earthquakes is not limited by the volume injected but rather by whatever it is that limits earthquake magnitudes on tectonic faults (geometry, prestress, etc.).

It is possible that the moment cap ultimately prohibits the occurrence of very large magnitude earthquakes and that the magnitude-frequency distribution is truncated at this upper limit. The consistency between the data and the expected Gutenberg-Richter sampling statistics (Test 1), demonstrates that any upper limit has been reached only rarely, if at all. In order to truly test these competing models, we need cases where the most probable maximum magnitude predicted by the sampling statistics actually exceeds the moment cap limit. Equating equation (3) with the moment magnitude limit from *McGarr* [2014], $M_w = (2/3)\log_{10}M_0 - 6$, with $M_0 = G\Delta V$, and assuming a typical seismogenic index $\Sigma = -1.5$, the crossover occurs at $\sim M6$ or an injection volume of about 3×10^7 m^3 into a single connected volume.

Until we have a sufficient number of such high-volume injection experiments, where the sampling statistics actually predict that earthquakes larger than the moment cap are expected, we must treat the deterministic cap on induced earthquake magnitudes as an untested hypothesis.

4.3. Implications for Forecasting the Largest Induced Earthquakes

The implications of the sample size hypothesis for seismic hazard are both positive and negative. On the one hand, the site-specific productivity of induced earthquakes (i.e., the seismogenic index) can be employed to

calculate the probability of a large earthquake, using existing probabilistic machinery for seismic hazard analysis, or to calibrate physics-based simulations of the interaction between fluids and a stochastic set of faults or earthquake nucleation sites [*Gischig and Wiemer*, 2013]. The linear scaling of number with injected volume (Figure 8) suggests that the number of future induced earthquakes can be forecast based on projected injection volumes and observations of N versus V in the past. In general, if an operation is not triggering small earthquakes, the probability of triggering large, damaging earthquakes is small.

Also on the positive side is the observation that the most likely maximum size at low injection volumes is apparently smaller than the moment cap prediction, at least for the high-profile sites collected in Figure 1. This is partly due to the fact that the b value at many injection sites appears to be somewhat larger than 1—with a median in this study of around 1.2 (Table 2)—which reduces the rate at which the expected largest earthquake grows with sample size (equations (1) and (5)). Higher than average b value may indeed be common to high-pressure fracturing operations [*Wyss*, 1973; *Grünthal*, 2014]. As a case in point, the 2013 to the present swarm of earthquakes in northern Oklahoma has a b value around 1.7. Despite the occurrence of over 300 M 3.5 or greater earthquakes since the start of 2014, the expected maximum is only M 5.0 (the largest to date has been a M 5.1). If b were in fact 1, we would expect to have had approximately 10 earthquakes above M 5.0, with an expected maximum of M 6.0.

On the downside, the statistical model holds that there is nothing intrinsic to the physics of induced—as opposed to tectonic—earthquakes that prevents them from exceeding a given magnitude. In the example of northern Oklahoma, the statistical model still predicts about a 2% chance of an earthquake above M 6 for every 300 earthquakes above M 3.5. Large earthquakes may be exceedingly rare in a statistical framework, but with enough time, even rare events are possible.

We should emphasize that the preceding statement is not a prediction. In the statistical model, the magnitude of a given earthquake is independent of all others in the sample. This means that the probability of drawing a large magnitude from the distribution is constant, regardless of how many draws have been conducted in the past. (No matter how many times a coin has come up heads in previous tosses, the probability of coming up tails on the next toss does not increase.) The fact that we have had >1400 $M \geq 3$ earthquakes in Oklahoma so far, without any above M 6, does not mean that an M 6 has now become more likely. The probability of seeing at least one M 6 earthquake among the next 1400 $M \geq 3$ earthquakes is the same as it was for the previous 1400.

The memorylessness of the sample size hypothesis cuts both ways; however, in that we cannot assume that there is no risk of a larger earthquake just because we are early in the lifetime of an injection well. While the rate of smaller earthquakes may be the best indicator of the probability of a large one, a large earthquake can occur with very little prior induced seismicity, as was seen in the case of the 2011 M 5.6 Prague earthquake.

5. Conclusion

The fundamental question in this paper is whether there is substantial evidence that the limit on induced earthquake magnitudes is smaller than the limit on similarly located tectonic earthquakes. We have framed this question as whether the largest observed induced earthquakes are any smaller or larger than we should have expected simply from the sampling statistics and the number of "draws" from the Gutenberg-Richter distribution of earthquake magnitudes.

We designed three tests to evaluate this possibility and find that the induced earthquake data pass them all: (1) The maximum observed magnitudes are consistent with the sampling statistics of the Gutenberg-Richter distribution with no upper bound. (2) The largest earthquakes are randomly distributed within the sequences rather than increasing in size with time/volume. (3) The number of induced earthquakes—not the cumulative moment—is proportional to the volume injected.

Given that the largest observed earthquakes are exactly as large as expected given the sampling statistics, we should be very cautious about physical models that conclude that the largest *possible* earthquake is already present in the rather sparse observations.

The discussion regarding induced earthquakes has moved from causality to mitigation. While there is little evidence that the maximum possible magnitude can be inferred from the data, there is considerable evidence that probabilistic hazard assessment is appropriate for induced seismicity. In particular, the rate of

triggered small earthquakes can be used to forecast the rate of large earthquakes, just like for tectonic environments. Adapting to changes in the rate due to changes in injection practices may present some difficulty, but this issue could likely be overcome with better access to current and anticipated injection totals.

Appendix A: Order Statistics of the MFD

This appendix describes the derivation of the most likely largest earthquake in a sample of independent and identically distributed magnitudes with no intrinsic upper limit on the magnitude.

A1. Distribution of Magnitudes

We start with the magnitude-frequency distribution of earthquakes [*Gutenberg and Richter*, 1944], which states that the number of earthquakes with magnitude M larger than some value m goes as

$$N(M \geq m) = N(M \geq M_c)10^{-b(m-M_c)} \tag{A1}$$

where M_c is a minimum threshold magnitude, such that $m \geq M_c$. This leads to the cumulative density function (cdf)

$$F_M(m) = 1 - 10^{-b(m-M_c)} \tag{A2}$$

and probability density function (pdf)

$$f_M(m) = b\ln 10 \cdot 10^{-b(m-M_c)}, \tag{A3}$$

with support $M_c \leq m$. In this paper we assume no upper bound on the support. For a more general treatment with a finite upper bound, see for instance *Holschneider et al*. [2011].

A2. Distribution of the Maximum Magnitude

Consider a random sample of size N. The probability that the largest observed magnitude $M_{\max}$ is smaller than or equal to some magnitude m is the same as the probability that all magnitudes M in the sample are smaller than m,

$$P(M_{\max} \leq m) = \prod_{i=1}^{N} P(M \leq m), \tag{A4}$$

or in terms of the cumulative density function

$$F_{M_{\max}}(m|N) = [F_M(m)]^N. \tag{A5}$$

Taking the derivative of the cumulative density (A5) with respect to m gives the probability density function for the maximum magnitude

$$f_{M_{\max}}(m|N) = N f_M(m)[F_M(m)]^{N-1}. \tag{A6}$$

The expectation of the maximum magnitude is not necessarily defined for the case of an unbounded distribution, so we use the mode, or most probable maximum magnitude, designated $\widehat{M}_{\max}$. Substituting (A2) and (A3) into (A6) and maximizing the probability density function (A6) with respect to m gives the mode

$$\widehat{M}_{\max} = M_c + \frac{1}{b}\log_{10}(N). \tag{A7}$$

Both the expectation (where it exists) and the median of the maximum magnitude are somewhat larger than the mode (A7) because the distribution is heavy tailed.

A shortcut to $\widehat{M}_{\max}$ can be found by setting $N = 1$ in (A1), which gives the magnitude at which we expect exactly one event. This shortcut is typically taken without acknowledging the correspondence to the mode of the distribution.

A3. Probability Bounds on the Maximum Magnitude

Probability bounds on the maximum observed magnitude can be found by inverting the cumulative density function (A5). For simplicity, let q be the value of the cdf at magnitude $m = \widehat{M}_q$. Substituting (A2) into (A5) and rearranging for $\widehat{M}_q$ gives

$$\widehat{M}_q = M_c - \frac{1}{b}\log_{10}\left(1 - q^{1/N}\right). \tag{A8}$$

Taking the difference of (A8) and (A7) removes the parameter M_c.

$$\widehat{M}_q = \widehat{M}_{\max} - \frac{1}{b}\log_{10}\left[N\left(1 - q^{1/N}\right)\right]. \tag{A9}$$

In the limit of large N or $q \sim 1$, the term $q^{1/N}$ can be approximated as $1 + \ln(q^{1/N})$. Substituting this into (A9) leads to the limiting case $\widehat{M}_q = \widehat{M}_{\max} - b^{-1}\log_{10}(-\ln(q))$.

A4. Conditioning the Sample Count on the Order of the Largest Earthquake

As described in the text, since N prior to the largest event is necessarily smaller than the total sample size N_{tot}, the naïve prediction $\widehat{M}_{\max}(N)$ must be smaller than the total sample prediction $\widehat{M}_{\max}(N_{tot})$. Here we derive the distribution of the difference between the true maximum magnitude $M_{\max}(N_{tot})$ and the naïve prediction $\widehat{M}_{\max}(N)$.

Define the difference between the true sample maximum and the naïve prediction as

$$\Delta M_{\max} = M_{\max}(N_{tot}) - \widehat{M}_{\max}(N), \tag{A10}$$

where N can take any value between 1 and N_{tot}. $M_{\max}(N_{\text{tot}})$ is the familiar maximum magnitude with distribution given by (A6) and $\widehat{M}_{\max}(N)$ is now a random variable found by taking equation (A7) with N distributed uniform from $[1, N_{\text{tot}}]$.

The pdf of $\Delta M_{\max}$ is obtained by substituting $\Delta M_{\max}$ (A10) in place of m in (A6) and then summing the joint distribution of ($\Delta M_{\max}$, N) over all possible values of N (marginalizing with respect to N);

$$f_{\Delta M_{\max}}(\Delta m|N_{tot}) = \frac{1}{N_{tot}}\sum_{N=N_{\min}}^{N_{tot}} f_{M_{\max}}\left(\Delta m + \widehat{M}_{\max}(N)|N_{tot}\right). \tag{A11}$$

Notice that the lower limit of the summation is not $N = 1$. This is due to the constraint $M_{\max} \geq M_c$, which limits the possible values of $\Delta M_{\max}$. Substituting the limit $M_{\max} = M_c$ into (A10) and combining with (A7) gives the lower limit on the number as

$$N_{\min} = 10^{-b\Delta m}, \tag{A12}$$

which is rounded up in practice.

Combining (A2), (A3), and (A6) into (A11) and simplifying, we obtain the distribution of the true maximum around the naïve prediction given by (A7)

$$f_{\Delta M_{\max}}(\Delta m|N_{tot}) = b\ln 10 \cdot 10^{-b\Delta m}\sum_{N=N_{\min}}^{N_{tot}}\frac{1}{N}\left[1 - \frac{1}{N}10^{-b\Delta m}\right]^{N_{tot}-1}, \tag{A13}$$

which is equation (6) in the main text. The expectation of $\Delta M_{\max}$ is given by

$$\langle \Delta M_{\max} \rangle = \frac{1}{b}\left[\log_{10}(N_{tot}) - \frac{1}{N_{tot}}\sum_{N=1}^{N_{tot}}\log_{10}(N)\right], \tag{A14}$$

which has the limit $1/b\log_{10}(e)$ for large N_{tot}, as can be shown by replacing the discrete summation in (A14) with an integral.

Acknowledgments

This paper benefitted from reviews and comments by Andrea Llenos, Morgan Moschetti, Associate Editor Martha Savage, and two anonymous reviewers. The earthquake data in this study are publically available in the referenced publications, except for the matched-filter catalogs for Harrison and Youngstown, OH, which are courtesy of P. Friberg and W.-Y. Kim, respectively. Any use of trade, firm, or product names is for descriptive purposes only and does not imply endorsement by the U.S. Government.

References

Ake, J., K. Mahrer, D. O'Connell, and L. Block (2005), Deep injection and closely monitored induced seismicity at Paradox Valley, Colorado, *Bull. Seismol. Soc. Am.*, *95*(2), 664–683, doi:10.1785/0120040072.

Aki, K. (1965), Maximum likelihood estimate of b in the formula log $N = a - bM$ and its confidence limits, *Bull. Earthquake Res. Inst.*, *43*, 237–239.

Asanuma, H., N. Soma, H. Kaieda, Y. Kumano, T. Izumi, K. Tezuka, H. Niitsuma, and D. Wyborn (2005), Microseismic monitoring of hydraulic stimulation at the Australian HDR project in Cooper Basin Proc. World Geothermal Congress, Antalya, Turkey 24-29 April 2005.

Bachmann, C. E., S. Wiemer, J. Woessner, and S. Hainzl (2011), Statistical analysis of the induced Basel 2006 earthquake sequence: Introducing a probability-based monitoring approach for enhanced geothermal systems, *Geophys. J. Int.*, *186*(2), 793–807.

Baisch, S., R. Weidler, R. Voros, D. Wyborn, and L. de Graaf (2006), Induced seismicity during the stimulation of a geothermal HFR reservoir in the Cooper Basin, Australia, *Bull. Seismol. Soc. Am.*, *96*, 2242–2256.

Baisch, S., R. Vörös, R. Weidler, and D. Wyborn (2009), Investigation of fault mechanisms during geothermal reservoir stimulation experiments in the Cooper Basin, Australia, *Bull. Seismol. Soc. Am.*, *99*(1), 148–158.

Baisch, S., R. Vörös, E. Rothert, H. Stang, R. Jung, and R. Schellschmidt (2010), A numerical model for fluid injection induced seismicity at Soultz-sous-Forêts, *Int. J. Rock Mech. Min. Sci.*, *47*(3), 405–413.
Baisch, S., E. Rothert, H. Stang, R. Vörös, C. Koch, and A. McMahon (2015), Continued geothermal reservoir stimulation experiments in the Cooper Basin (Australia), *Bull. Seismol. Soc. Am.*, *105*(1), 198–209, doi:10.1785/0120140208.
Block, L. V., C. K. Wood, W. L. Yeck, and V. M. King (2014), The 24 January 2013 M_L 4.4 earthquake near Paradox, Colorado, and its relation to deep well injection, *Seismol. Res. Lett.*, *85*(3), 609–624, doi:10.1785/0220130188.
Brodsky, E., and N. J. van der Elst (2014), The uses of dynamic earthquake triggering, *Annu. Rev. Earth Planet. Sci.*, *42*, 317–339, doi:10.1146/annurev-earth-060313-054648.
Charlety, J., N. Cuenot, L. Dorbath, C. Dorbath, H. Haessler, and M. Frogneux (2007), Large earthquakes during hydraulic stimulations at the geothermal site of Soultz-sous-Forêts, *Int. J. Rock Mech. Min. Sci.*, *44*(8), 1091–1105.
Clauset, A., C. R. Shalizi, and M. E. J. Newman (2009), Power-law distributions in empirical data, *SIAM Rev.*, *51*(4), 661–703.
Davis, S. D., and C. Frohlich (1993), Did (or will) fluid injection cause earthquakes? Criteria for a rational assessment, *Seismol. Res. Lett.*, *64*, 207–224.
de Pater, C. J., and Baisch S. (2011), Geomechanical study of Bowland Shale seismicity: Synthesis report, prepared for Cuadrilla Resources Ltd. [Available at www.cuadrillaresources.com/wp-content/uploads/2012/02/Geomechanical-Study-of-Bowland-Shale-Seismicity_02-11-11.pdf.]
Dieterich, J. (1994), A constitutive law for rate of earthquake production and its application to earthquake clustering, *J. Geophys. Res.*, *99*(B2), 2601–2618, doi:10.1029/93JB02581.
Eaton, D. W., J. Davidsen, P. K. Pedersen, and N. Boroumand (2014), Breakdown of the Gutenberg-Richter relation for microearthquakes induced by hydraulic fracturing: Influence of stratabound fractures, *Geophys. Prospect.*, *62*, 806–818, doi:10.1111/1365-2478.12128.
Eisner, L., Janská E., Opršal I., and Matoušek P. (2011), Seismic analysis of the events in the vicinity of the Preese Hall well, Seismik S.R.O, Final report prepared for Cuadrilla Ltd. [Available at www.cuadrillaresources.com/wp-content/uploads/2012/02/Geomechanical-Study-Appendix-3-2.11.2011.pdf.]
Evans, D. M. (1966), The Denver area earthquake and the Rocky Mountain Arsenal disposal well, *Mt. Geol.*, *3*(1), 23–36.
Friberg, P. A., G. M. Besana-Ostman, and I. Dricker (2014), Characterization of an earthquake sequence triggered by hydraulic fracturing in Harrison County, Ohio, *Seismol. Res. Lett.*, *85*(6), 462, doi:10.1785/0220140127.
Frohlich, C. (2012), Two-year survey comparing earthquake activity and injection-well locations in the Barnett Shale, Texas, *Proc. Natl. Acad. Sci. U.S.A.*, *109*(35), 13,934–13,938.
Frohlich, C., C. Hayward, B. Stump, and E. Potter (2011), The Dallas-Fort Worth earthquake sequence: October 2008 through May 2009, *Bull. Seismol. Soc. Am.*, *101*(1), 327–340, doi:10.1785/0120100131.
Frohlich, C., W. Ellsworth, W. A. Brown, M. Brunt, J. Luetgert, T. MacDonald, and S. Walter (2014), The 17 May 2012 *M*4.8 earthquake near Timpson, East Texas: An event possibly triggered by fluid injection, *J. Geophys. Res. Solid Earth*, *119*, 581–593, doi:10.1002/2013JB010755.
Gischig, V. S., and S. Wiemer (2013), A stochastic model for induced seismicity based on non-linear pressure diffusion and irreversible permeability enhancement, *Geophys. J. Int.*, *194*(2), 1229–1249.
Goebel, T. H. W., E. Hauksson, F. Aminzadeh, and J.-P. Ampuero (2015), An objective method for the assessment of fluid injection-induced seismicity and application to tectonically active regions in central California, *J. Geophys. Res. Solid Earth*, doi:10.1029/2015JB011895.
Goodfellow, S. D., M. H. B. Nasseri, S. C. Maxwell, and R. P. Young (2015), Hydraulic fracture energy budget: Insights from the laboratory, *Geophys. Res. Lett.*, *42*, 3179–3187, doi:10.1002/2015GL063093.
Grünthal, G. (2014), Induced seismicity related to geothermal projects versus natural tectonic earthquakes and other types of induced seismic events in Central Europe, *Geothermics*, *52*, 22–35, doi:10.1016/j.geothermics.2013.09.009.
Gutenberg, B., and C. F. Richter (1944), Frequency of earthquakes in California, *Bull. Seismol. Soc. Am.*, *4*, 185–188.
Hallo, M., I. Oprsal, L. Eisner, and M. Y. Ali (2014), Prediction of magnitude of the largest potentially induced seismic event, *J. Seismol.*, *18*(3), 421–431.
Hanks, T. C., and H. Kanamori (1979), A moment magnitude scale, *J. Geophys. Res.*, *84*(B5), 2348–2350, doi:10.1029/JB084iB05p02348.
Häring, M. O., U. Schanz, F. Ladner, and B. C. Dyer (2008), Characterization of the Basel 1 enhanced geothermal system, *Geothermics*, *37*(5), 469–495.
Helmstetter, A., Y. Y. Kagan, and D. D. Jackson (2005), Importance of small earthquakes for stress transfers and earthquake triggering, *J. Geophys. Res.*, *110*, B05S08, doi:10.1029/2004JB003286.
Holland, A. A. (2013), Earthquakes triggered by hydraulic fracturing in south-central Oklahoma, *Bull. Seismol. Soc. Am.*, *103*(3), 1784–1792, doi:10.1785/0120120109.
Holschneider, M., G. Zöller, and S. Hainzl (2011), Estimation of the maximum possible magnitude in the framework of a doubly truncated Gutenberg-Richter model, *Bull. Seismol. Soc. Am.*, *101*(4), 1649–1659, doi:10.1785/0120100289.
Holschneider, M., G. Zoller, R. Clements, and D. Schorlemmer (2014), Can we test for the maximum possible earthquake magnitude? *J. Geophys. Res. Solid Earth*, *119*, 2019–2028, doi:10.1002/2013JB010319.
Hornbach, M. J., et al. (2015), Causal factors for seismicity near Azle, Texas, *Nat. Commun.*, *6*, 6728, doi:10.1038/ncomms7728.
Horton, S. (2012), Disposal of hydrofracking waste fluid by injection into subsurface aquifers triggers earthquake swarm in central Arkansas with potential for damaging earthquake, *Seismol. Res. Lett.*, *83*(2), 250–260, doi:10.1785/gssrl.83.2.250.
Hsieh, P. A., and J. S. W. Bredehoeft (1981), A reservoir analysis of the Denver earthquakes—A case study of induced seismicity, *J. Geophys. Res.*, *86*, 903–920, doi:10.1029/JB086iB02p00903.
Ishimoto, M., and K. Iida (1939), Observations of earthquakes registered with the microseismograph constructed recently, *Bull. Earthq. Res. Inst. Univ. Tokyo*, *17*, 443–478.
Jost, M. L., T. Büßelberg, Ö. Jost, and H.-P. Harjes (1998), Source parameters of injection-induced microearthquakes at 9 km depth at the KTB Deep Drilling site, Germany, *Bull. Seismol. Soc. Am.*, *88*(3), 815–832.
Keranen, K. M., H. M. Savage, G. A. Abers, and E. S. Cochran (2013), Potentially induced earthquakes in Oklahoma, USA: Links between wastewater injection and the 2011 M_w 5.7 earthquake sequence, *Geology*, *41*(6), 699–702.
Keranen, K. M., M. Weingarten, G. A. Abers, B. A. Bekins, and S. Ge (2014), Sharp increase in central Oklahoma seismicity since 2008 induced by massive wastewater injection, *Science*, *345*(6195), 448–451, doi:10.1126/science.1255802.
Kim, W.-Y. (2013), Induced seismicity associated with fluid injection into a deep well in Youngstown, Ohio, *J. Geophys. Res. Solid Earth*, *118*, 3506–3518, doi:10.1002/jgrb.50247.
Llenos, A. L., and A. J. Michael (2013), Modeling earthquake rate changes in Oklahoma and Arkansas: Possible signatures of induced seismicity, *Bull. Seismol. Soc. Am.*, *103*(5), 2850–2861, doi:10.1785/0120130017.
McGarr, A. (1976), Seismic moments and volume changes, *J. Geophys. Res.*, *81*(8), 1487–1494, doi:10.1029/JB081i008p01487.

McGarr, A. (2014), Maximum magnitude earthquakes induced by fluid injection, *J. Geophys. Res. Solid Earth*, *119*, 1008–1019, doi:10.1002/2013JB010597.

Mignan, A. (2016), Static behavior of induced seismicity, *Nonlinear Processes Geophys.*, *23*, 107–113, doi:10.5194/npg-23-107-2016.

Mignan, A., L. Danciu, and D. Giardini (2015), Reassessment of the maximum fault rupture length of strike-slip earthquakes and inference on M_{max} in the Anatolian Peninsula, Turkey, *Seismol. Res. Lett.*, *86*(3), 890–900.

Mignan, A., D. Landtwing, P. Kästli, B. Mena, and S. Wiemer (2015b), Induced seismicity risk analysis of the 2006 Basel, Switzerland, Enhanced Geothermal System project: Influence of uncertainties on risk mitigation, *Geothermics*, *53*, 133–146, doi:10.1016/j.geothermics.2014.05.007.

National Research Council (2013), *Induced Seismicity Potential in Energy Technologies*, 225 pp., National Academies Press, Washington, D. C.

Petersen, M. D., Mueller C. S., Moschetti M. P., Hoover S. M., Rubinstein J. L., Llenos A. L., and Michael A. J. (2015), Incorporating induced seismicity in the 2014 United States National Seismic Hazard Model: Results of the 2014 workshop and sensitivity studies, *U.S. Geol. Surv. Open File Rep.*, 2015-1070, doi:10.3133/ofr20151070.

Rubinstein, J. L., W. L. Ellsworth, A. McGarr, and H. M. Benz (2014), The 2001–present induced earthquake sequence in the Raton Basin of northern New Mexico and southern Colorado, *Bull. Seismol. Soc. Am.*, *104*, 2162–2181, doi:10.1785/0120140009.

Seeber, L., J. G. Armbruster, and W. Y. Kim (2004), A fluid-injection-triggered earthquake sequence in Ashtabula, Ohio: Implications for seismogenesis in stable continental regions, *Bull. Seismol. Soc. Am.*, *94*(1), 76–87.

Segall, P., and S. Lu (2015), Injection-induced seismicity: Poroelastic and earthquake nucleation effects, *J. Geophys. Res. Solid Earth*, *120*, 5082–5103, doi:10.1002/2015JB012060.

Shapiro, S. A., C. Dinske, and J. Kummerow (2007), Probability of a given-magnitude earthquake induced by a fluid injection, *Geophys. Res. Lett.*, *34*, L22314, doi:10.1029/2007GL031615.

Shapiro, S. A., C. Dinske, and C. Langenbruch (2010), Seismogenic index and magnitude probability of earthquakes induced during reservoir fluid stimulations, *Leading Edge*, *29*(3), 304–309.

Shapiro, S. A., O. S. Krüger, C. Dinske, and C. Langenbruch (2011), Magnitudes of induced earthquakes and geometric scales of fluid-stimulated rock volumes, *Geophysics*, *76*(6), WC55–WC63, doi:10.1190/GEO2010-0349.1.

Shi, Y., and B. A. Bolt (1982), The standard error of the magnitude-frequency *b* value, *Bull. Seismol. Soc. Am.*, *72*, 1677–1687.

Sumy, D., E. Cochran, K. M. Keranen, M. Wei, and G. A. Abers (2014), Observations of static Coulomb stress triggering of the November 2011 *M* 5.7 Oklahoma earthquake sequence, *J. Geophys. Res. Solid Earth*, *119*, 1904–1923, doi:10.1002/2013JB010612.

van der Elst, N. J., H. M. Savage, K. M. Keranen, and G. A. Abers (2013), Enhanced remote earthquake triggering at fluid-injection sites in the midwestern United States, *Science*, *341*(164), 164–167, doi:10.1126/science.1238948.

van Thienen-Visser, K., and J. N. Breunese (2015), Induced seismicity of the Groningen gas field: History and recent developments, *Leading Edge*, *34*(6), 664–671, doi:10.1190/tle34060664.1.

Wang, H. F. (2000), *Theory of Linear Poroelasticity*, Princeton Univ. Press, Princeton.

Wyss, M. (1973), Towards a physical understanding of the earthquake frequency distribution, *Geophys. J. Int.*, *31*(4), 341–359.

Zoback, M. D., and H. P. Harjes (1997), Injection-induced earthquakes and crustal stress at 9 km depth at the KTB deep drilling site, Germany, *J. Geophys. Res.*, *102*(B8), 18,477–18,491, doi:10.1029/96JB02814.